ELSEVIER

Fluid Dynamics Research 29 (2001) 227–250

FLUID DYNAMICS RESEARCH

Numerical study of stably stratified flows over a two-dimensional hill in a channel of finite depth ☆

Takanori Uchida *, Yuji Ohya

Research Institute for Applied Mechanics, Kyushu University, 6-1 Kasuga-koen, Kasuga-city, Fukuoka 816-8580, Japan

Received 20 December 2000; received in revised form 25 April 2001; accepted 30 June 2001

Abstract

Stably stratified flows over a two-dimensional hill in a channel of finite depth are investigated numerically at a Reynolds number of 2000, which is based on the uniform upstream velocity U and the hill height h. As a first step, we assume a free-slip condition on the ground, both upstream and downstream of the hill, and impose a no-slip condition only on the hill surface. Such a configuration corresponds to that of the previous towing tank experiments and numerical studies. For strong stratification ($1 < K = NH/\pi U \leqslant 2$), the present numerical results confirmed that the flow around the hill is intrinsically unsteady, which is manifested very clearly as periodic oscillations in the drag coefficient C_d on the hill, and emphasize the following features, where N is the buoyancy frequency and H is the channel depth. For $1.1 \leqslant K \leqslant 1.7$, columnar disturbances with mode $n = 1$ are dominant so that the flow around the hill shows a persistent periodic unsteadiness. This flow unsteadiness is mainly due to the periodic shedding of upstream advancing columnar disturbances with mode $n = 1$ with a clockwise circulation. For $1.8 \leqslant K \leqslant 2$, as columnar disturbances with mode $n = 2$ become dominant, the flow around the hill rapidly reaches an almost steady state. In addition, through the calculations with the blockage ratio $H/h = 6, 10$ and corresponding $\mathrm{Re} = 20$, 100 and 2000, it is found that the normalized periods of C_d oscillations have a strong dependence on both the H/h and Re. As a next step, to investigate the flow around the hill under real atmospheric situations, we have performed calculations under imposition of a no-slip condition on the ground, particularly focusing on the effect of stable stratifications on the unsteady separated–reattached flow behind the hill. The flow around the hill exhibits different behavior over the whole range $0 \leqslant K \leqslant 2$, corresponding to the difference in the boundary condition on the ground. For $0 \leqslant K \leqslant 0.9$, the vortex shedding from the separation bubble behind the hill occurs. For $K = 1$ and 1.1, the vortex shedding is strongly suppressed so that the flow around the hill rapidly reaches an almost steady state. Under strong stratification ($1 < K \leqslant 2$), although lee waves are excited downstream of the hill, the vortex shedding clearly exists. For $1.2 \leqslant K \leqslant 1.5$, the flow field with a vortex shedding shows an approximately steady state, corresponding to the stationary lee wave. It is much more likely that there is no significant change in the approaching flow just ahead of the hill, because the change in the columnar disturbances with mode $n = 1$ is very small. Only when $1.6 \leqslant K \leqslant 2$ does the

☆ This is an English version translated from two Japanese papers published in Nagare (1998) 17(1) 45–56, and (1999) 18(5) 308–320.

* Corresponding author. Fax: +81-92-583-7779.

E-mail address: takanori@riam.kyushu-u.ac.jp (T. Uchida).

PII: S0169-5983(01)00025-9

flow around the hill become unsteady. However, the rate of the periodic change in the separation bubble is very small. These flow mechanisms for $1.6 \leqslant K \leqslant 2$ are almost the same as those discussed in the prior numerical results.

Keywords: Direct numerical simulation; Finite-difference method; Stably stratified flows; Finite depth; Two-dimensional hill; Unsteady flow; Columnar disturbance; Separated–reattached flow

1. Introduction

Stably stratified flows over topography have attracted great interest from not only fluid mechanicians but also engineers in a variety of fields. For example, investigations of pollutant transport and dispersion in stably stratified flows over complex terrain are critical for the protection of air quality, because industrial plants and other sources of air pollution frequently locate within or near complex terrain. The stable stratification effect strongly influences plume behaviors over complex terrain. Depending on the release height and stratified conditions, plumes may be observed to be entrained into rotors or vortices of numerous types, or to be transported long distances with little or no dispersion.

We consider two-dimensional internal waves excited topographically in stably stratified flows in a channel of finite depth. Under these conditions, the fluid layer is bounded above by a horizontal rigid lid and below by a two-dimensional surface-mounted obstacle. Therefore, all upward propagating energy of internal waves is reflected downward, and is trapped in this fluid layer. According to the linear theory (e.g. Turner, 1973), internal waves in a channel of finite depth have a continuous spectrum in the horizontal with wave number k_x and a discrete spectrum in the vertical with wave number $k_z = n\pi/H$. The flow around topography is characterized by the parameter $K(=NH/\pi U)$, where N is the buoyancy frequency, H is the channel depth and U is the uniform upstream velocity. The linear dispersion relation for internal waves with the vertical mode number n is

$$\omega^2 \left(k_x^2 + \frac{n^2\pi^2}{H^2} \right) - N^2 k_x^2 = 0, \tag{1a}$$

where ω is the angular frequency. The horizontal phase velocity $C_{p_x}(k_x)$ of these waves is given by

$$C_{p_x}(k_x) = \frac{\omega}{k_x} = \frac{N}{\{k_x^2 + (n\pi/H)^2\}^{1/2}}, \tag{1b}$$

and the horizontal group velocity $C_{g_x}(k_x)$ by

$$C_{g_x}(k_x) = \frac{\partial\omega}{\partial k_x} = \frac{N(n\pi/H)^2}{\{k_x^2 + (n\pi/H)^2\}^{3/2}}. \tag{1c}$$

From Eqs. (1b) and (1c), $C_{p_x}(k_x)$ and $C_{g_x}(k_x)$ take their maximum values in the limit of $k_x \to 0$ (columnar disturbance), at which they are given by

$$C_{p_x}(0) = C_{g_x}(0) = \frac{NH}{n\pi}. \tag{1d}$$

This columnar disturbance, which is a manifestation of long internal waves and has an almost horizontal motion relative to the uniform flow, propagates upstream at the speed of

$$C_{p_x}(0) - U = \frac{NH}{n\pi} - U = \left(\frac{K}{n} - 1 \right) U, \tag{1e}$$

with respect to topography. From Eq. (1e), for the cases of $0 \leqslant K \leqslant 1$, since the flow is supercritical to all the wave modes (i.e., $C_{p_x}(k_x)$ and $C_{g_x}(k_x)$ of the columnar disturbance are less than U), no upstream columnar motion occurs. In this study we call these ranges of K the weak stratification. On the other hand, for the cases of $1 < K \leqslant 2$, the flow becomes subcritical to the mode $n=1$ (i.e., $C_{p_x}(k_x)$ and $C_{g_x}(k_x)$ are greater than U) so that the wave with mode $n=1$ begins to propagate upstream of topography in the form of a columnar disturbance at the speed of $(K-1)U$. We call these ranges of K the strong stratification. It should be noted here that $K(=NH/\pi U)$ is physically interpreted as the ratio of the maximum horizontal phase or group velocity (NH/π) of the columnar disturbance with mode $n=1$ to the uniform upstream velocity U (see Eq. (1d)).

Stably stratified flows over two-dimensional topography in a channel of finite depth have been the subject of extensive study since the pioneering work of Long (1953, 1955). For this special but important class of flows, there have been many theoretical (e.g. McIntyre, 1972; Janowitz, 1981), experimental (e.g. Castro et al., 1990; Baines, 1995) and numerical (e.g. Castro, 1989; Hanazaki, 1989a, b; Paisley and Castro, 1994a; Lamb, 1994; Rottman et al., 1996) findings. The most striking feature of these findings has been the unsteadiness in the flow around topography for strong stratification ($1 < K \leqslant 2$). Castro et al. (1990) found in their towing tank experiments that an obstacle drag in linearly stratified flows shows a persistent periodic oscillation for $1.4 < K < 2$. Similar phenomena have been confirmed in a number of numerical simulations under the same conditions (Hanazaki, 1989a, b; Paisley and Castro, 1994a; Lamb, 1994; Rottman et al., 1996). To date, these numerical simulations have been of two types: viscous laminar flow simulations with low Reynolds numbers of less than 100 (Castro, 1989; Hanazaki, 1989a, b; Paisley and Castro, 1994a) and inviscid flow simulations (Lamb, 1994; Rottman et al., 1996). However, there have been a limited number of numerical studies with high Reynolds numbers (Paisley et al., 1994b; Uchida and Ohya, 1997). The possible mechanism of this periodic flow unsteadiness has been discussed (Castro et al., 1990; Hanazaki, 1989a, b; Paisley and Castro, 1994a; Rottman et al., 1996). Castro et al. (1990) discussed that variations in the C_d are a consequence of those in the effective value of K upstream of the obstacle, which are associated with changes in the strength of columnar disturbances. Hanazaki (1989a, b) asserted that time-dependent oscillations in the strength of columnar disturbances (eddies) detaching upstream from the obstacle lead to those in the C_d. He also suggested that the strength of each columnar mode approaches a certain constant value that depends on K and is not zero as time proceeds. Paisley and Castro (1994a) offered an explanation for these C_d oscillations with the assumption that the role of the body in tuning the flow was an important factor. Namely, it is much more likely that unsteady behavior in the C_d is a result of non-linear processes. Based on the assumption that the periodic flow unsteadiness around topography is mainly due to the internal wave that remains oscillating in the neighborhood of topography for the longest time, Rottman et al. (1996) derived the period T_n of this most persistent wave as a function of K from the linear theory (e.g. Turner, 1973). It is then given by

$$T_n = \frac{2}{n}\left[\left(\frac{K}{n}\right)^{2/3} - 1\right]^{-3/2}\frac{H}{U}. \tag{1f}$$

Such waves should have a group velocity equal in magnitude but opposite in direction to the approaching flow speed, and propagate upstream of topography at the speed of $\{(K/n)^{2/3} - 1\}U$. They suggested that the agreement between predictions by Eq. (1f) and measured periods of the C_d

oscillations from their numerical results and the previous experimental (Castro et al., 1990) and numerical (Paisley and Castro, 1994a; Lamb, 1994) studies is quite good, in spite of the fact that in a stratified viscous fluid, there is a boundary layer separation in the lee of topography. However, a complete account of the flow unsteadiness around the hill under high Reynolds numbers is not given. Furthermore, the effect of a variety of factors, such as the blockage ratio (H/h), the Reynolds number and the boundary condition on the ground, on the flow around the hill still remains unclear.

In the present numerical studies, we describe the results of linearly stratified flows over a two-dimensional hill at a relatively high Reynolds number of 2000. A direct numerical simulation (DNS), which involves the numerical solution of the Navier–Stokes equation without any turbulent model, is performed by using a finite-difference method (FDM). In particular, we assume a free-slip condition on the ground, both upstream and downstream of the hill, and impose a no-slip condition only on the hill surface. Such a configuration corresponds to that of the aforementioned towing tank experiments (Castro et al., 1990; Baines, 1995) and numerical studies (Castro, 1989; Hanazaki, 1989a, b; Paisley and Castro, 1994a, Paisley et al., 1994b). Particular emphasis is placed on the mechanisms of the flow unsteadiness around the hill for strong stratification ($1 < K \leqslant 2$) at a relatively high Reynolds number of 2000. The effects of a variety of factors, such as the blockage ratio (H/h) and the Reynolds number, on the flow around the hill are also discussed. As a next step, to investigate the flow around the hill under real atmospheric situations, we perform calculations with a no-slip condition on the ground, particularly focusing on the effect of stable stratifications on the unsteady separated–reattached flow behind the hill.

2. Computational details

2.1. Governing equations

We consider a linearly stratified flow of incompressible and non-diffusive fluid past a two-dimensional hill in a channel of finite depth. Fig. 1 shows the schematic view of the flow configuration employed. It consists of a streamwise length $L = 400h$ and a vertical depth $H = 6h$, where h is the hill height. In order to simulate a bounded fluid, an absorbing region (with enhanced friction) is usually installed near the inflow boundary to eliminate the influence of upstream propagating perturbations from the hill. In this study, the inflow boundary is sufficiently long ($320h$ in all the calculations) that the flow in the neighborhood of the hill is fully developed without an absorbing

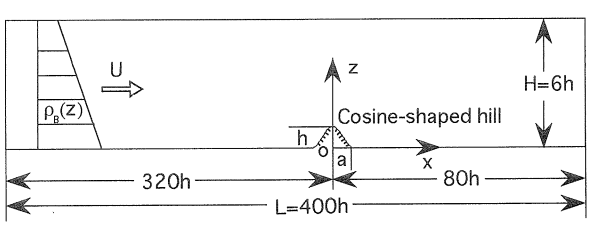

Fig. 1. Schematic view of the flow configuration.

region. For the geometry of the hill, a simple cosine function is chosen with a profile given by

$$h(x) = 0.5 \times \{1 + \cos(\pi x/a)\}, \tag{2a}$$

where the hill geometry parameter a is set at 1. Under the Boussinesq approximation, the dimensional governing equations for unknown variables $u_i = (u, w)$, ρ' and p' consist of the continuity, Navier–Stokes and density equations. The equations are written in the gradient form as follows:

$$\frac{\partial u_i}{\partial x_i} = 0, \tag{2b}$$

$$\frac{\partial u_i}{\partial t} + u_j \frac{\partial u_i}{\partial x_j} = -\frac{1}{\rho_0}\frac{\partial p'}{\partial x_i} + \frac{\mu}{\rho_0}\frac{\partial^2 u_i}{\partial x_j \partial x_j} - \frac{\rho' g \delta_{i3}}{\rho_0}, \tag{2c}$$

$$\frac{\partial \rho'}{\partial t} + u_j \frac{\partial \rho'}{\partial x_j} = -w\frac{\mathrm{d}\rho_B}{\mathrm{d}z}. \tag{2d}$$

ρ' and p' are the perturbation density and pressure defined as

$$\rho' = \rho - \rho_B, \quad p' = p - p_B,$$

where $x_i = (x, z)$ are the physical coordinate components, $u_i = (u, w)$ are the corresponding physical velocity components, ρ_0 is the reference density, μ is the viscosity coefficient and g is the acceleration due to gravity. The variables of ρ_B and p_B, which satisfy the hydrostatic equilibrium $\mathrm{d}p_B/\mathrm{d}z = -\rho_B g$, are the undisturbed basic distributions at the inflow boundary, and ρ_B decreases linearly with height, namely, $\mathrm{d}\rho_B/\mathrm{d}z = -1$. The subscripts i, j take values of 1, 3 to denote the streamwise (x) and vertical (z) directions, respectively. Non-dimensionalizing all variables using the uniform upstream velocity U, hill height h and reference density ρ_0, we have the following three dimensionless equations:

$$\frac{\partial u_i}{\partial x_i} = 0, \tag{3a}$$

$$\frac{\partial u_i}{\partial t} + u_j \frac{\partial u_i}{\partial x_j} = -\frac{\partial p}{\partial x_i} + \frac{1}{\mathrm{Re}}\frac{\partial^2 u_i}{\partial x_j \partial x_j} - \frac{\rho \delta_{i3}}{\mathrm{Fr}^2}, \tag{3b}$$

$$\frac{\partial \rho}{\partial t} + u_j \frac{\partial \rho}{\partial x_j} = w. \tag{3c}$$

These governing equations include two dimensionless parameters, i.e., the Reynolds number $\mathrm{Re}(= \rho_0 U h/\mu)$ and the Froude number $\mathrm{Fr}(= U/Nh)$, where N is the buoyancy frequency defined as $N^2 = -(g/\rho_0)(\mathrm{d}\rho_B/\mathrm{d}z)$. It should be noted here that for the stratified flow of finite depth not only Re and Fr but also $K(= NH/\pi U)$, which contains the channel depth H, is a parameter necessary to determine the character of internal waves. Since K is rewritten as $K = H/\pi h\,\mathrm{Fr}$, it is determined by H/h when Fr is a known number. In other words, K reflects the effect of boundary conditions though it does not appear explicitly in the governing equations. We summarize the numerical results in terms of K, rather than Fr.

2.2. Simulation methods and parameters

In order to simulate the flow around the hill with high accuracy, a generalized curvilinear coordinate system ($x = x(\xi, \zeta)$, $z = z(\xi, \zeta)$) is employed. Hence, the original governing equations (3a)–(3c)

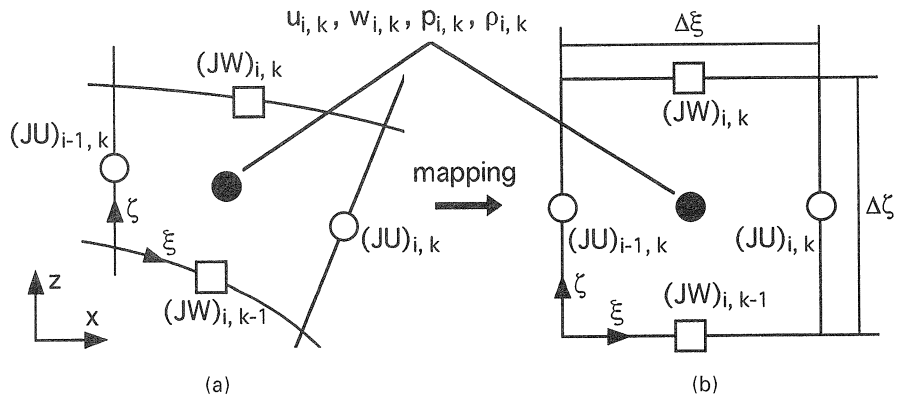

Fig. 2. Collocated grid in a generalized curvilinear coordinate system.

in the physical space are transformed to the computational space as follows:

$$\frac{1}{J}\left[\frac{\partial(JU^j)}{\partial\xi^j}\right]=0, \tag{4a}$$

$$\frac{\partial u_i}{\partial t}+\frac{1}{J}\left[(JU^j)\frac{\partial u_i}{\partial\xi^j}\right]=-\frac{\partial\xi^j}{\partial x_i}\frac{\partial p}{\partial\xi^j}+\frac{1}{\mathrm{Re}}\tilde{\nabla}^2u_i-\frac{\rho\delta_{i3}}{\mathrm{Fr}^2}, \tag{4b}$$

$$\frac{\partial\rho}{\partial t}+\frac{1}{J}\left[(JU^j)\frac{\partial\rho}{\partial\xi^j}\right]=w. \tag{4c}$$

The Jacobian and the contravariant velocity components are given by

$$J=\left|\frac{\partial x_i}{\partial\xi^j}\right|, \tag{4d}$$

$$U^j=\frac{\partial\xi^j}{\partial x_i}u_i. \tag{4e}$$

The governing equations (4a)–(4c) in the computational space are approximated by a finite-difference method (FDM) based on a collocated grid. A full description of a numerical method using a collocated grid can be found in Zang et al. (1994). Here something should be said about a variable arrangement of a collocated grid. The physical velocity components, pressure and density are defined at the center of a cell, while the contravariant velocity components multiplied by the Jacobian are defined at the midpoint on their corresponding cell surfaces, as shown in Fig. 2. The coupling algorithm of physical velocity components and pressure is based on an extension of the fractional step method (Kim and Moin, 1985) to the incompressible stratified flow. Therefore, the pressure Poisson equation derived from Eq. (4b) is solved by the successive overrelaxation (hereafter SOR) method. The iterative solution of the pressure Poisson equation is the most time-consuming part of the overall solution procedure. In the previous numerical studies (Ohya et al., 1992; Uchida and Ohya, 1997), we used a regular grid in which all variables were defined at the same location for a computational grid. Therefore, when the grid resolution was too high to resolve the fine scales, we always experienced an inefficient convergence of the SOR method. The results of the present numerical method

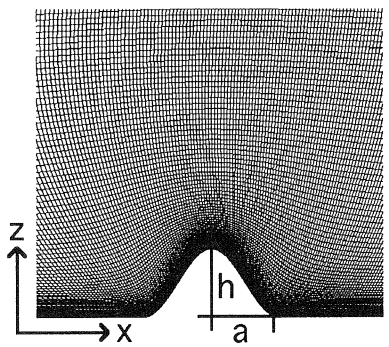

Fig. 3. Computational grid near a hill.

based on a collocated grid were considerably improved over those of the previous method based on a regular grid. Accordingly, the former method was much more efficient than the latter in terms of CPU time. The Euler explicit method with a first-order accuracy is used for time advancement in Eqs. (4b) and (4c). As for the discretization of spatial derivatives in the governing equations, all spatial derivatives except for the convective terms are approximated by a second-order central scheme. For the convective terms, a modified third-order upwind scheme is used. For example, a part of the x-component is expressed as

$$\frac{1}{J}\left[(JU)\frac{\partial f}{\partial \xi}\right]_{i,k} \cong \frac{1}{J}[\overline{\overline{(JU)}^{\xi}\delta_{\xi} f}^{\xi}]_{i,k} + |U_{i,k}|\frac{u_{i+2,k} - 4u_{i+1,k} + 6u_{i,k} - 4u_{i-1,k} + u_{i-2,k}}{4\,\Delta\xi}. \tag{4f}$$

The first term of the right-hand side of Eq. (4f) is an appropriate fourth-order central scheme for a collocated grid (Kajishima et al., 1997). The second term is a fourth-derivative error term, the so-called artificial numerical viscosity, that can minimize the numerical dissipation of velocities and density while avoiding the appearance of any numerical oscillations (Kawamura et al., 1986). The signs of $-\xi$ and δ_{ξ} represent an interpolation operator and a finite-difference operator, respectively. The formulas are defined as

$$[\delta_{\xi} f]_{i,k} = \frac{-f_{i+3/2,k} + 27(f_{i+1/2,k} - f_{i-1/2,k}) + f_{i-3/2,k}}{24\,\Delta\xi}, \tag{4g}$$

$$[\bar{f}^{\xi}]_{i,k} = \frac{-f_{i+3/2,k} + 9(f_{i+1/2,k} + f_{i-1/2,k}) - f_{i-3/2,k}}{16}, \tag{4h}$$

where f is an arbitrary function and $\Delta\xi$ is the grid scale ($\Delta\xi = 1$). The number of grid points is 501×101 in the x- and z-directions. The computational grid near the hill is shown in Fig. 3. The grid points in the physical space are sufficiently concentrated toward the hill surface and ground. The vertical smallest grid spacing at the hilltop is $3 \times 10^{-3}h$. To examine the accuracy of the numerical results, a grid refinement study was also conducted. A very fine grid, which has 1001×201 grid points in the x- and z-directions, was used. Comparisons between the numerical results with 501×101 grid points and those with 1001×201 grid points show that changes in the grid resolutions are negligibly small on the numerical results so that we expect that the present calculations with 501×101 grid

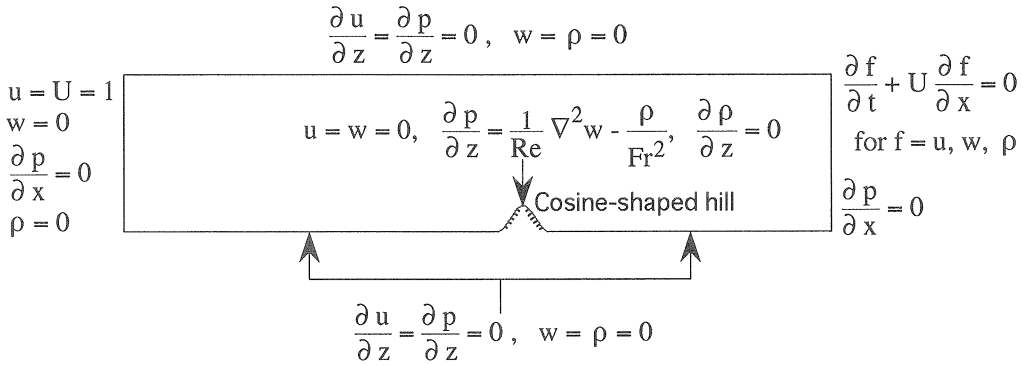

Fig. 4. Boundary conditions.

points are free from the grid dependence. The boundary conditions are shown in Fig. 4. The condition of $\partial/\partial z = 0$ on the upper boundary and ground except for the hill surface is a free-slip condition. A no-slip condition is imposed only on the hill surface ($|x| \leqslant a$). Such physical conditions closely match the previous towing tank experiments (Castro et al., 1990; Baines, 1995) and numerical studies (Castro, 1989; Hanazaki, 1989a, b; Paisley and Castro, 1994a, Paisley et al., 1994b). Impulsive-start, which represents a suddenly accelerated flow from rest, is employed for an initial condition. We calculate the flow around the hill at a relatively high Reynolds number of 2000 for a wide range of K ($0 \leqslant K \leqslant 3$). A non-dimensional time increment is fixed at $\Delta t = (1 \text{ or } 2) \times 10^{-3}$.

3. Results for free-slip conditions

3.1. *Weak stratification* ($0 \leqslant K \leqslant 1$)

Fig. 5 shows the instantaneous streamlines around a hill for weak stratification ($0 \leqslant K \leqslant 1$) at a non-dimensional time $t = 200$. A stationary vortex behind the hill is observed, different from the real three-dimensional stratified flows over topography. Its size is suppressed as K increases. For $K = 0.8$ and 1, a stationary lee wave with long wavelength appears downstream of the hill. This lee wave can be more clearly observed in Fig. 6(c) and (d). The stationary vortex gradually elongates as time proceeds for all the cases, but we will not discuss this phenomenon (Chernyshenko and Castro, 1993) in detail because it is beyond the scope of this study. A further investigation of the developing flow field around the hill reveals that the rate of the gradual elongation in the size of the stationary vortex for $K = 1$ is significantly smaller than that of the other cases of $K = 0$–0.8. This is likely due to the existence of the long lee wave for $K = 1$.

Fig. 6 shows the corresponding perturbation streamlines ($\Delta\psi$), which are depicted by the perturbation velocity components ($\Delta u = u - U$ and $\Delta w = w$). These $\Delta\psi$ make clear the existence of lee waves and columnar disturbances propagating upstream of the hill. For $K = 0$ and 0.5, $\Delta\psi$ represent the stationary vortex behind the hill, as shown in Fig. 5(a) and (b). As K approaches 1, the front of $\Delta\psi$ above the hill moves upstream of the hill (see arrows), but the systematic upstream propagation

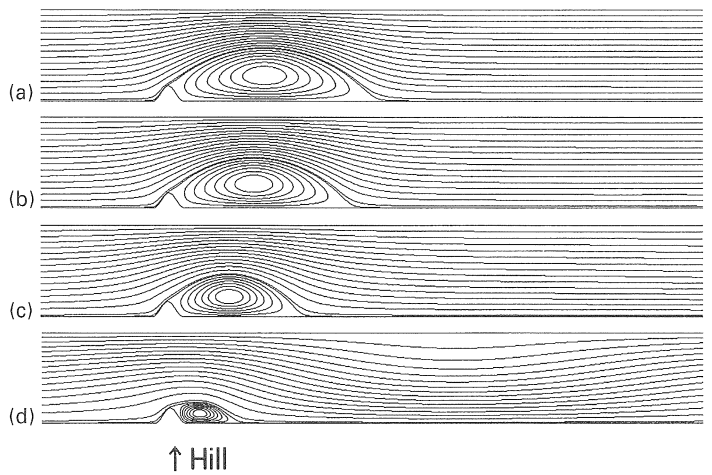

Fig. 5. Instantaneous streamlines around a hill for weak stratification ($0 \leqslant K \leqslant 1$) at a non-dimensional time $t = 200$, $\mathrm{Re} = 2000$: (a) $K = 0$; (b) $K = 0.5$; (c) $K = 0.8$; (d) $K = 1$. Dotted lines indicate counter clockwise circulations in Fig. 9(b)–(d).

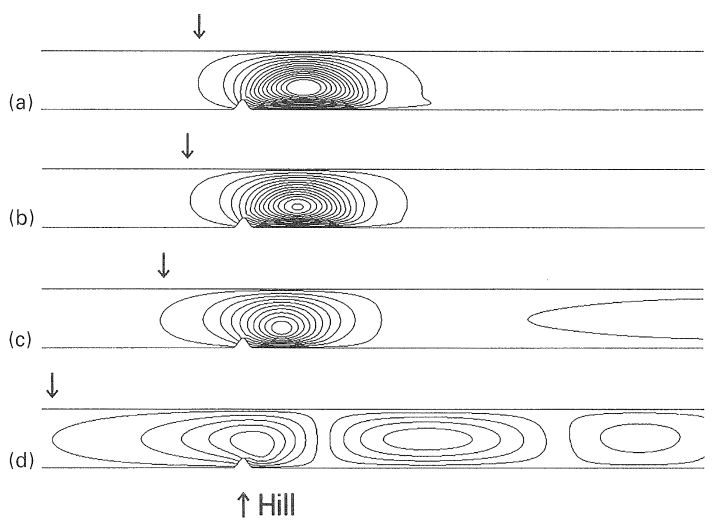

Fig. 6. Perturbation streamlines ($\Delta\psi$) corresponding to Fig. 5, $-4 \leqslant \Delta\psi \leqslant 2$: (a) $K = 0$; (b) $K = 0.5$; (c) $K = 0.8$; (d) $K = 1$.

of columnar disturbances is not yet observed. For $K = 0.8$ and 1, $\Delta\psi$ are seen downstream of the hill, implying the existence of lee waves.

Fig. 7 shows the time history of drag coefficient C_d on the hill over a period of integration $0 \leqslant t \leqslant 500$. The behavior in the C_d for all the cases suggests that the flow around the hill reaches an almost steady state. To be precise, however, these C_d variations do not reach any K-dependent constant values, reflecting the gradual elongation in the size of the stationary vortex behind the hill, as pointed out by Hanazaki (1989a).

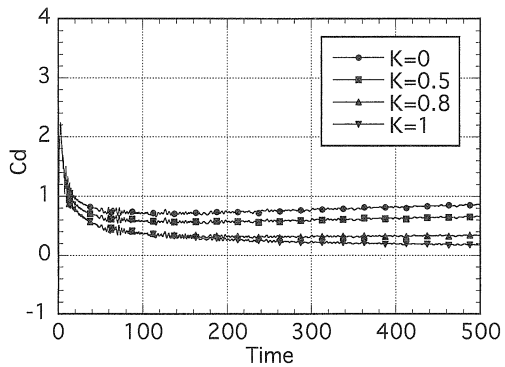

Fig. 7. Time history of drag coefficient C_d on a hill for weak stratification ($0 \leqslant K \leqslant 1$), Re = 2000.

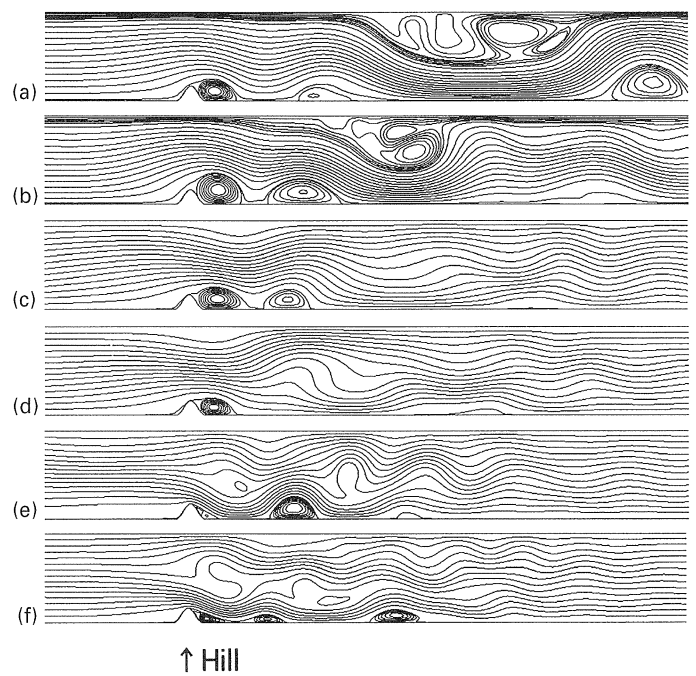

Fig. 8. Instantaneous streamlines around a hill for strong stratification ($1 < K \leqslant 2$), $K = 2.5$ and 3, Re = 2000: (a) $K = 1.3$, $t = 313$; (b) $K = 1.5$, $t = 314$; (c) $K = 1.8$, $t = 60$; (d) $K = 2$, $t = 60$; (e) $K = 2.5$, $t = 50$; (f) $K = 3$, $t = 50$.

3.2. *Strong stratification* ($1 < K \leqslant 2$), $K = 2.5$ *and 3*

Fig. 8 shows the instantaneous streamlines around a hill for strong stratification ($1 < K \leqslant 2$), $K = 2.5$ and 3. For all the cases, a lee wave is excited downstream of the hill and its wavelength is gradually shortened as K increases. The upward and downward flows in the lee wave motion induce eddy regions on both the downstream ground (Fig. 8(a)–(c), (e) and (f)) and upper boundary (Fig. 8(a) and (b)). In this study we refer to these eddy regions, which are induced by the lee wave motion, as the rotor. Moreover, a wave breaking is observed for $K = 2.5$ and 3.

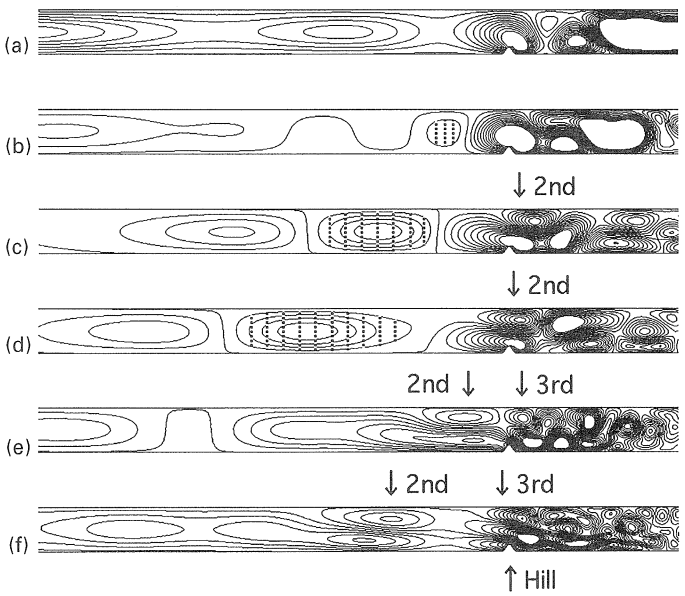

Fig. 9. Perturbation streamlines ($\Delta\psi$) corresponding to Fig. 8, $-1 \leqslant \Delta\psi \leqslant 1$: (a) $K = 1.3$; (b) $K = 1.5$; (c) $K = 1.8$; (d) $K = 2$; (e) $K = 2.5$; (f) $K = 3$.

Fig. 9 shows the corresponding perturbation streamlines ($\Delta\psi$). The most striking feature in Fig. 9 is that closed $\Delta\psi$ also appears upstream of the hill, indicating the existence of upstream advancing columnar disturbances. The wave with mode $n = 1$ begins to propagate upstream in the form of a columnar disturbance. The detaching of the eddy is seen since the strong and weak parts appear, in turn, in the upstream advancing columnar disturbances with mode $n = 1$ (Hanazaki, 1989a). For $K = 1.3$ and 1.5, in which the columnar disturbance with mode $n = 1$ is dominant, the mode $n = 1$ eddy is detached at successively shorter periods as K becomes larger (see also Fig. 11). For $K \geqslant 1.8$, columnar disturbances with mode $n = 2$ elongate upstream of the hill (Baines, 1979; Hanazaki, 1989a) and for $K \geqslant 2.5$, those with mode $n = 3$ are seen near the hill. It should be noted that columnar disturbances with mode $n = 1$, generated as detaching eddies, have only a clockwise circulation for $K = 1.3$, while for $K \geqslant 1.5$, they have both clockwise and counterclockwise circulations (see also Fig. 11). A detaching eddy with a clockwise circulation is generated from the hill, while the one with a counterclockwise circulation is generated from a rotor attached to the upper boundary near the hill. Thus, a rotor seems to behave as the origin of columnar disturbances (Baines, 1995). According to the linear theory (e.g. Turner, 1973), the propagation speed of columnar disturbances is given by Eq. (1e). The values obtained from the present calculations are consistent with those by Eq. (1e) for all the cases.

Fig. 10 shows the time history of drag coefficient C_d on the hill for strong stratification ($1 < K \leqslant 2$) over a period of integration $0 \leqslant t \leqslant 500$. There are two interesting features in this figure. First, for $K = 1.3$ and 1.5, the persistent periodic C_d oscillations, which have an approximately constant amplitude and period, are observed. Especially for $K = 1.5$, they have a quite large amplitude. Secondly, for $K = 1.8$ and 2, the C_d oscillations rapidly decay after about $t = 200$. The former implies that the persistent periodic unsteadiness exists in the flow around the hill. The latter shows that the flow

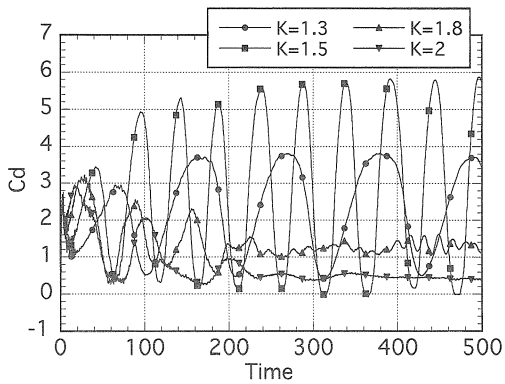

Fig. 10. Time history of drag coefficient C_d on a hill for strong stratification ($1 < K \leqslant 2$), $\mathrm{Re} = 2000$.

unsteadiness around the hill rapidly decays after about $t = 200$. Paisley and Castro (1994a) also reported persistent periodic oscillations in the C_d for $1.3 \leqslant K \leqslant 1.6$ and decaying oscillations in the C_d for $1.7 \leqslant K \leqslant 2$.

3.3. *Mechanism of the periodic flow unsteadiness around the hill for* $1 < K \leqslant 2$

First, we offer the origin of the persistent periodic flow unsteadiness around the hill for strong stratification ($1 < K \leqslant 2$) as follows. To investigate more clearly the relation between the flow unsteadiness and the behavior of columnar disturbances (especially for the disturbance with mode $n = 1$), we calculated the time history of u_1 and u_2 at an upstream point of the hill (i.e., $x = -2h$) over a period of integration $0 \leqslant t \leqslant 500$. It is then defined by

$$u_n = \frac{2}{H} \int_0^H \left(\frac{\Delta u}{U} \right) \cos\left(\frac{n\pi z}{H} \right) \mathrm{d}z. \tag{5}$$

The results are shown in Fig. 11, together with variations in the C_d on the hill. These u_1 and u_2 values make clear the strength of individual upstream advancing columnar modes with $n = 1$ and 2. Here, u_1 with a negative value corresponds to a columnar disturbance of mode $n = 1$ with a clockwise circulation. On the other hand, u_1 with a positive value corresponds to a columnar disturbance of mode $n = 1$ with a counterclockwise circulation. At first glance, we notice that variations in the C_d on the hill are precisely in phase with those in the u_1 for all the cases. In other words, the periods of C_d oscillations are certainly consistent with those of the shedding of upstream advancing columnar disturbances with mode $n = 1$. Therefore, these results indicate the following in regard to the origin of the persistent periodic flow unsteadiness around the hill. It may be driven by the periodic shedding of upstream advancing columnar disturbances, which are generated from the hill, of mode $n = 1$ with a clockwise circulation, as proposed by Hanazaki (1989a, b). Consequently, this event leads to a periodic modification in the flow just ahead of the hill, as we describe in the following paragraph.

Next, we concentrate on the reason why variations in the C_d on the hill take their high and low values. For this purpose, we examine the flow field around the hill for $K = 1.5$ in more detail. Fig. 12 shows the instantaneous streamlines at low- and high-C_d states, respectively. There are several large differences in the flow pattern around the hill between two states. First, we can see lee waves with

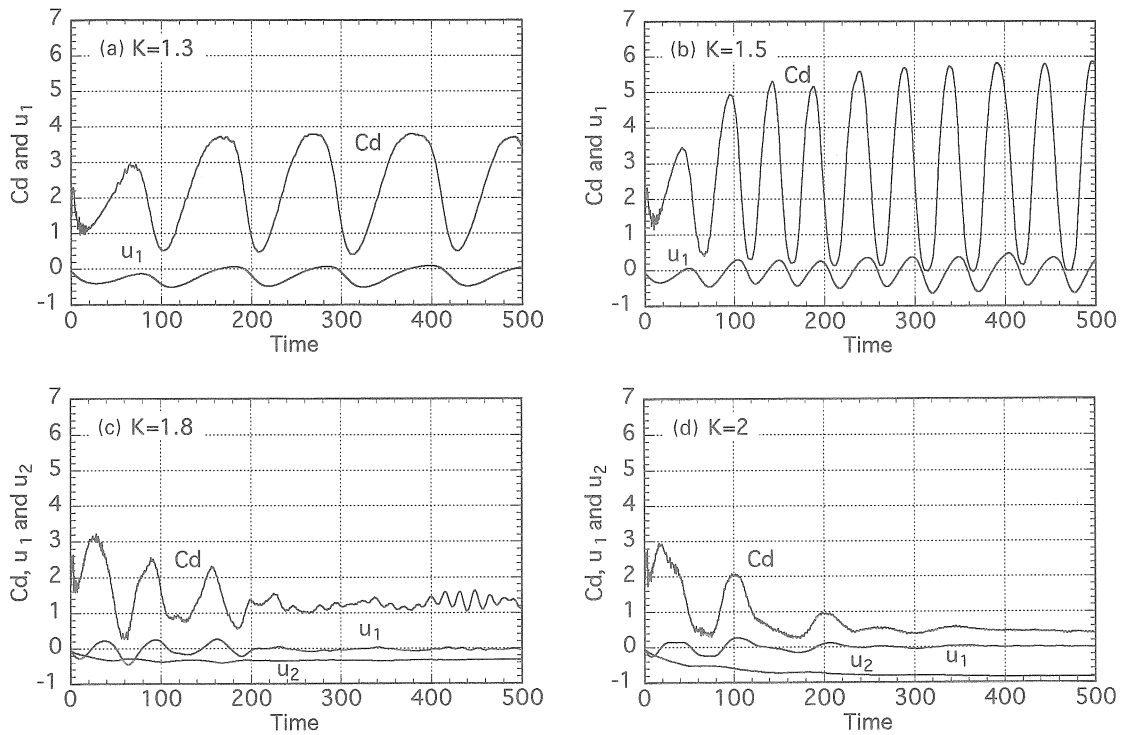

Fig. 11. Time history of drag coefficient C_d on a hill, columnar mode with $n=1$ (u_1) and mode with $n=2$ (u_2) for strong stratification ($1 < K \leqslant 2$), Re = 2000.

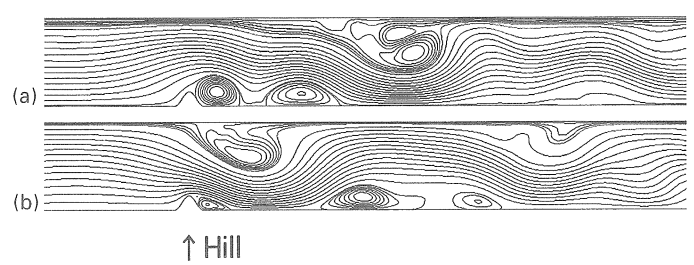

Fig. 12. Instantaneous streamlines around a hill for $K=1.5$, Re = 2000: (a) Low-C_d state, $t=314$; (b) High-C_d state, $t=339$.

a small amplitude over the hill at a low-C_d state in Fig. 12(a), while these waves are of a large amplitude at a high-C_d state in Fig. 12(b). Secondly, a large stationary vortex behind the hill is induced by the corresponding upward flow in the lee wave motion over the hill at a low-C_d state, whereas a small one is induced by the corresponding downward flow at a high-C_d state.

Fig. 13 shows the corresponding perturbation streamlines ($\Delta\psi$) and velocity vectors (Δu and Δw) in the vicinity of the hill at low- and high-C_d states. First, we note that a columnar disturbance (eddy) of mode $n=1$ with a clockwise circulation, indicated by an arrow, is just about to detach from the hill at a low-C_d state in Fig. 13(a), while this disturbance has just detached from the hill

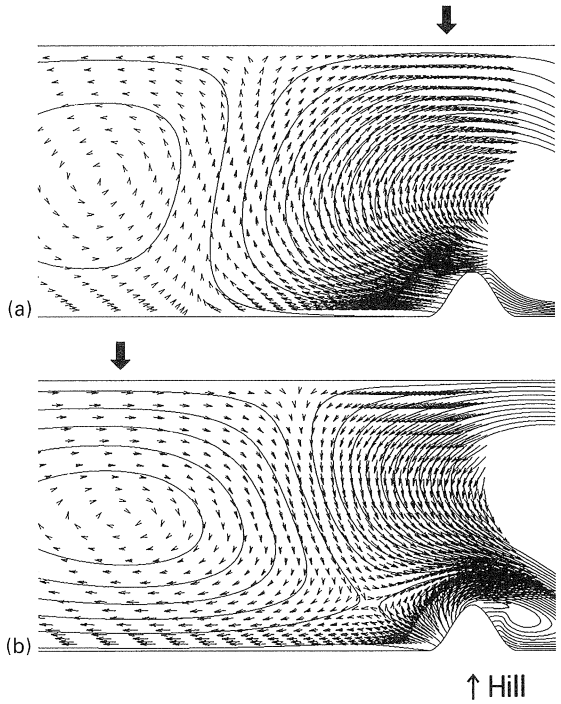

Fig. 13. Perturbation streamlines ($\Delta\psi$) and velocity vectors (Δu and Δw) corresponding to Fig. 12, $-1 \leqslant \Delta\psi \leqslant 1$: (a) Low-$C_d$ state; (b) High-C_d state.

at a high-C_d state in Fig. 13(b). Therefore, an upward flow is induced in front of the hill at a low-C_d state. On the other hand, a downward flow is induced in front of the hill at a high-C_d state. Immediately upstream of the hill, these upward and downward flows modify the approaching flow directly for the hill: the former tends to lift the approaching flow up; the latter tends to press it down. As a result, the curvature of the separated–reattached shear layer generating from the hill becomes small at a low-C_d state, while it becomes large at a high-C_d state. Since the base pressure of the hill is directly influenced by the curvature of the separated–reattached shear layer, C_d variations become low values due to the small curvature and high values due to the large curvature.

3.4. *Mechanism of decaying C_d oscillations for $1.8 \leqslant K \leqslant 2$*

Let us now examine the mechanism of decaying C_d oscillations for $1.8 \leqslant K \leqslant 2$. Fig. 14 shows the well-developed perturbation streamlines ($\Delta\psi$) for $K = 1.8$ and 2 at $t = 350$. Fig. 15 shows the corresponding streamlines. From Fig. 14, it is apparent that both clockwise and counterclockwise circulations are symmetrically arranged with reference to the horizontal center axis of the channel. This phenomenon manifests the appearance of columnar disturbances with mode $n = 2$. This wave contributes no fluctuations to the approaching flow, eventually leading the flow around the hill to be symmetric with respect to the horizontal center axis of the channel, as shown in Fig. 15. Accordingly, as time proceeds, namely, as columnar disturbances with mode $n = 1$ disappear and those with mode $n = 2$ become dominant instead, the flow around the hill rapidly reaches an almost steady state.

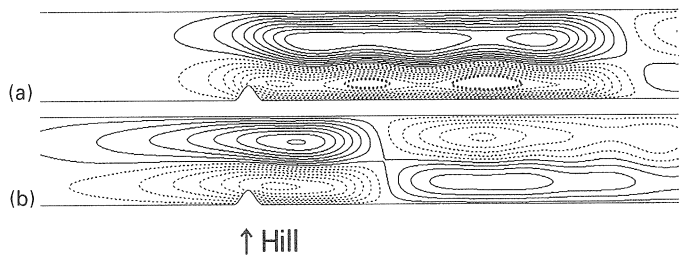

Fig. 14. Perturbation streamlines ($\Delta\psi$) around a hill at $t=350$, $\mathrm{Re}=2000$, $-1.3 \leqslant \Delta\psi \leqslant 1.3$: (a) $K=1.8$; (b) $K=2$. Dotted and full lines indicate clockwise and counterclockwise circulations, respectively.

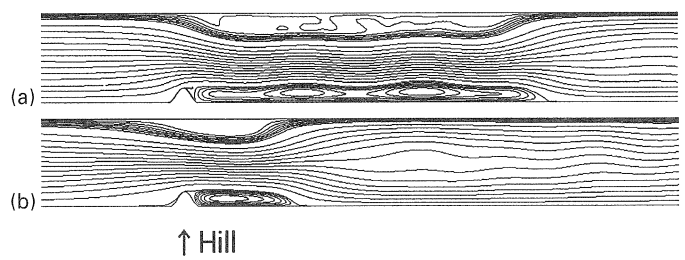

Fig. 15. Instantaneous streamlines corresponding to Fig. 14: (a) $K=1.8$; (b) $K=2$.

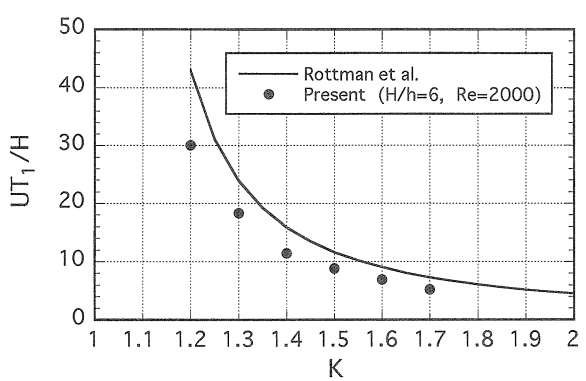

Fig. 16. Comparison between the normalized periods (UT_1/H) of persistent periodic C_d oscillations obtained from the present numerical results with $\mathrm{Re}=2000$ and the values predicted by Rottman et al. (1996) (i.e., Eq. (1f)).

3.5. *Effect of the blockage ratio and Reynolds number on the periodic flow unsteadiness*

There is a significant difference in the normalized periods (UT_1/H) of C_d oscillations between the values predicted by Rottman et al. (1996) (i.e., Eq. (1f)) and those obtained from the present calculations with $\mathrm{Re}=2000$. The comparison between two results is shown in Fig. 16. A distinct difference in the normalized periods of C_d oscillations is obviously found, especially for $K=1.2$. To further investigate this discrepancy, we examined the effect of the blockage ratio H/h and Reynolds number Re on the periodic flow unsteadiness around the hill.

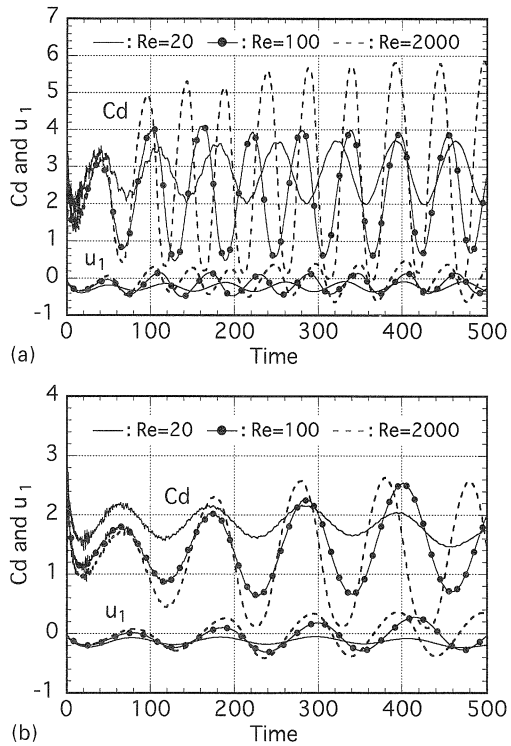

Fig. 17. Time history of drag coefficient C_d on a hill and columnar mode with $n=1$ (u_1) for $K=1.5$: (a) $H/h=6$, Re = 20, 100 and 2000; (b) $H/h=10$, Re = 20, 100 and 2000. The normalized period (UT_1/H) of C_d oscillations is about 11.5 (Re = 20), 10 (Re = 100) and 8.8 (Re = 2000) with $H/h=6$, compared to 11.6 by Eq. (1f). On the other hand, it is about 11.5 (Re = 20), 11.5 (Re = 100) and 10 (Re = 2000) with $H/h=10$.

Fig. 17 shows the time history of C_d and u_1 calculated from Eq. (5) over a period of integration $0 \leqslant t \leqslant 500$ for $K=1.5$, where $H/h=6$ and Re = 20, 100 and 2000 in Fig. 17(a), while $H/h=10$ and Re = 20, 100 and 2000 in Fig. 17(b). From Fig. 17, we can see several striking features as follows. For all the cases, despite the differences in the H/h and in the Re, the C_d variations are completely in phase with those in the u_1. Therefore, the periodic flow unsteadiness around the hill may be caused by the similar mechanism suggested in Figs. 12 and 13. For the individual blockage ratio, as the Reynolds number decreases, the normalized periods of C_d oscillations tend to reach an almost same value predicted by Eq. (1f). Furthermore, a comparison between Fig. 17(a) and (b) shows that as the blockage ratio becomes larger, the trend in approaching the predicted value by Eq. (1f) is remarkable at the same Reynolds number, especially for the case with Re = 2000. This is likely due to the inhibition of the non-linear effect on the periodic flow unsteadiness around the hill. Therefore, it is reasonable to conclude that in the present numerical results with $H/h=6$ and Re = 2000 the non-linear effect can be strongly enhanced, eventually leading to the differences between the predicted values by Eq. (1f). In particular, it is shown that the effect of the blockage ratio is relatively dominant, rather than the Reynolds number in the range $20 \leqslant \mathrm{Re} \leqslant 2000$. It should

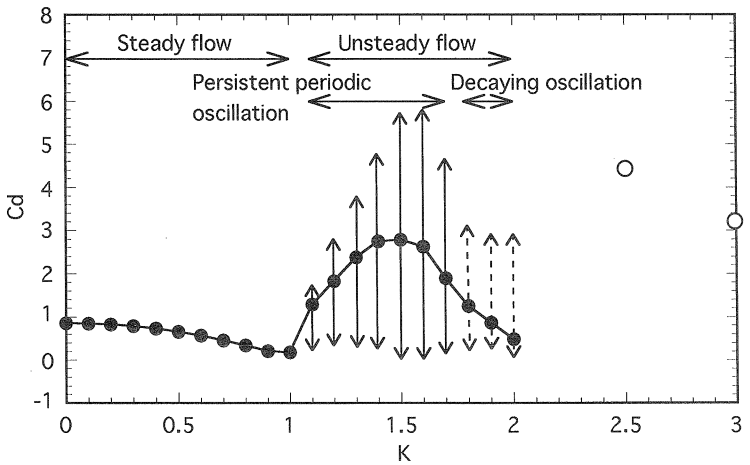

Fig. 18. Variations of drag coefficient C_d on a hill with K ($0 \leqslant K \leqslant 3$), $\mathrm{Re} = 2000$. Full and dotted lines indicate persistent and decaying C_d oscillations, respectively. In addition, the flow characteristics around the hill for $0 \leqslant K \leqslant 2$ are summarized. For $K = 2.5$ and 3, the flow around a hill becomes complicated.

be noted here that variations in the u_1 with $H/h = 10$ and $\mathrm{Re} = 20$ in Fig. 17(b) gradually reach a K-dependent constant value, as pointed out by Hanazaki (1989a, b).

3.6. *Variation in the drag coefficient C_d on the hill with K ($0 \leqslant K \leqslant 3$)*

Fig. 18 shows the time-averaged drag coefficient C_d on the hill for $0 \leqslant K \leqslant 3$. The arrows in the figure indicate the fluctuations from the time-mean values. We can see that C_d decreases locally at integral values of $K = 1$, 2 and 3. The overall trend in the behavior of C_d is almost similar to that obtained from the previous theoretical (Janowitz, 1981) and numerical (Castro, 1989; Hanazaki, 1989a, b; Paisley and Castro, 1994a) studies. Also in Fig. 18, flow characteristics around the hill for $0 \leqslant K \leqslant 2$ are summarized. The flow patterns can be classified into two regimes: the weak stratification ($0 \leqslant K \leqslant 1$), in which the flow around the hill approaches an almost steady state as time proceeds, mainly due to the generation of lee waves (especially for $K = 1$) and the strong stratification ($1 < K \leqslant 2$), in which the flow unsteadiness caused by the columnar disturbance is observed. Furthermore, the strong stratification ($1 < K \leqslant 2$) can be classified into two regimes. For $1.1 \leqslant K \leqslant 1.7$, columnar disturbances with mode $n = 1$ are dominant so that the flow around the hill shows a persistent periodic unsteadiness. For $1.8 \leqslant K \leqslant 2$, as columnar disturbances with mode $n = 1$ disappear and those with mode $n = 2$ become dominant instead, the flow around the hill rapidly reaches an almost steady state.

4. Results for no-slip conditions

As a next step, in order to investigate the flow around the hill under real atmospheric situations, we attempt calculations under imposition of a no-slip condition on the ground. Under these physical conditions, generally speaking, the flow over topography becomes sufficiently complicated owing to

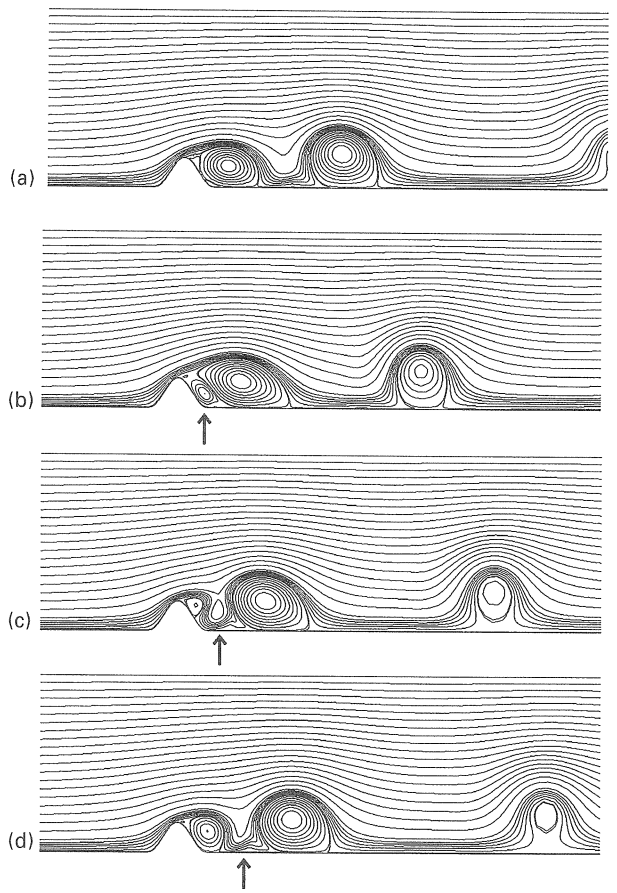

Fig. 19. Time sequence of streamlines covering one cycle of vortex shedding for $K = 0$, $\mathrm{Re} = 2000$: (a) $t = 148$; (b) $t = 152$; (c) $t = 155$; (d) $t = 157$.

the unsteady separated–reattached flow behind topography. In previous studies, we have attempted to clarify the effect of stable stratifications on the unsteady separated–reattached flow behind the surface-mounted obstacle at relatively high Reynolds numbers ($\mathrm{Re} = 2000$–7500) both experimentally and numerically (Ohya et al., 1992). However, the detailed flow features and mechanisms still remain unclear. To avoid a troublesome boundary layer effect, we employ a free-slip condition on the ground upstream of the hill, much as in our previous numerical study (Ohya et al., 1992). A no-slip condition is imposed on the hill surface ($|x| \leqslant a$) and the downstream of the hill.

4.1. Vortex shedding from the separation bubble generated behind the hill ($K = 0$)

Fig. 19 shows a time sequence of streamlines covering one cycle of vortex shedding for $K = 0$. The shear layer separating from the hill surface reattaches to the ground downstream of the hill and forms a separation bubble behind the hill (Fig. 19(a)). This separation bubble has a clockwise circulation. As time proceeds, the separation bubble gradually elongates in the streamwise direction.

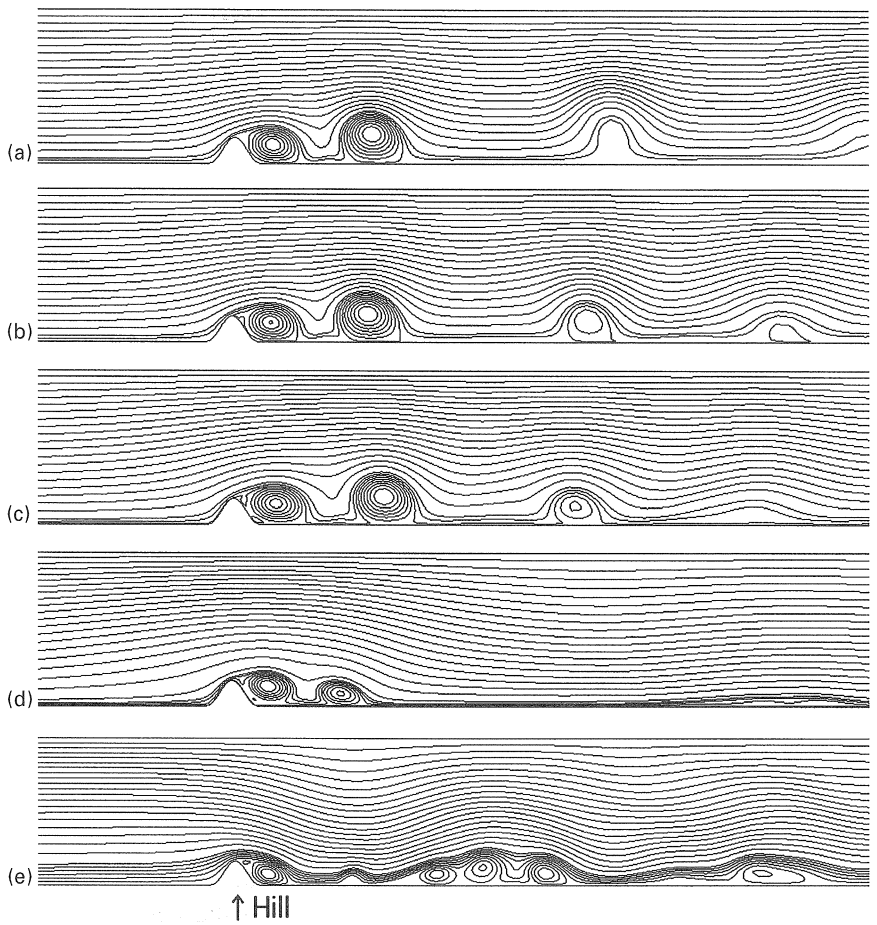

Fig. 20. Instantaneous streamlines around a hill for $0 \leqslant K \leqslant 1.3$, Re = 2000: (a) $K = 0$, $t = 148$; (b) $K = 0.5$, $t = 200$; (c) $K = 0.8$, $t = 151$; (d) $K = 1$, $t = 200$; (e) $K = 1.3$, $t = 200$.

Coincidentally, a secondary eddy with a counterclockwise circulation (see the arrow) is induced in the separation bubble (Fig. 19(b)). As the secondary eddy moves along the ground, a new separated shear layer from the hilltop begins to reattach to the downwind surface of the hill again (Fig. 19(c)). As a result, a first vortex (a separation bubble) is shed downstream of the hill (Fig. 19(d)).

4.2. *Flow characteristics with* K $(0 \leqslant K \leqslant 3)$

Fig. 20 shows the instantaneous streamlines around a hill for $0 \leqslant K \leqslant 1.3$. All of them, except for the case of $K = 1$, indicate approximately the same phase of vortex shedding. For $K = 0.5$ and 0.8, the stratification effect on the flow field cannot be seen near the downstream in the wake. Similar to the case of $K = 0$, the vortex shedding from the separation bubble occurs. For $K = 1$, the flow around the hill is markedly different from that observed in the cases of $K = 0$–0.8. That is, a stationary lee wave with long wavelength appears downstream of the hill so that the vortex shedding

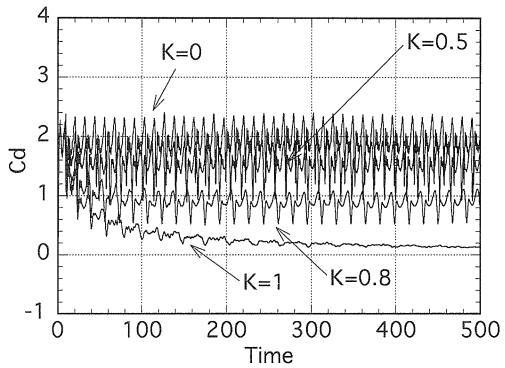

Fig. 21. Time history of drag coefficient C_d on a hill for weak stratification ($0 \leqslant K \leqslant 1$), Re = 2000.

is strongly suppressed. For $K = 1.3$, there are several significant differences in the flow around the hill, as distinct from the prior numerical result in Fig. 8(a). First, a stationary lee wave is excited, similar to our previous wind-tunnel experiment (Ohya et al., 1992). Secondly, an upward flow in the lee wave motion induces a rotor on the ground downstream of the hill. However, its size is remarkably smaller than that observed in the prior numerical result. Thirdly, no rotor that is induced by the downward flow in the lee wave motion is found on the upper boundary.

Fig. 21 shows the time history of the drag coefficient C_d on the hill over a period of integration $0 \leqslant t \leqslant 500$. The C_d variations for $K = 0-0.8$ show a regular fluctuation with a constant amplitude. It is apparent that there is periodic vortex shedding from the separation bubble behind the hill. For $K = 1$, the C_d oscillations rapidly decay after about $t = 100$ and reach an almost constant value. This phenomenon implies that due to the generation of the long lee wave, the vortex shedding is strongly suppressed so that the flow around the hill becomes an almost steady state. A further investigation of the C_d variations shows that small fluctuations are seen for all the cases. This can be attributed to the existence of the secondary eddy induced in the separation bubble behind the hill, as shown in Fig. 19.

Fig. 22 shows the time history of C_d, u_1 and u_2 over a period of integration $0 \leqslant t \leqslant 500$. For $K = 1.3$ and 1.5, different from Fig. 11(a) and (b), C_d variations show an almost steady state, corresponding to the stationary lee wave. It is much more likely that there is no significant change in the approaching flow just ahead of the hill, because the change in the u_1 is very small. For $K = 1.8$, the persistent periodic C_d oscillations are observed, different form Fig. 11(c). This may be due to the fact that the change in the u_1 is significantly dominant. For $K = 2$, C_d oscillations rapidly decay after about $t = 100$, similar to Fig. 11(d). Interestingly, we can see short-period oscillations in the C_d for all the cases, just as in Fig. 21. Namely, although lee waves are excited downstream of the hill, the vortex shedding from the separation bubble behind the hill clearly exists (see Fig. 23).

Fig. 23 shows the time-averaged drag coefficient C_d on the hill for $0 \leqslant K \leqslant 3$. The arrows in the figure indicate the fluctuations from the time-mean values. C_d decreases locally at integral values of $K = 1$, 2 and 3, similar to Fig. 18. Fig. 23 also summarizes the flow characteristics around the hill for $0 \leqslant K \leqslant 2$. The flow patterns can be classified into three regimes: Regime-A, in which the vortex shedding from the separation bubble generated behind the hill is dominant; Regime-B, in which the flow unsteadiness caused by the columnar disturbance cannot be observed; and Regime-C,

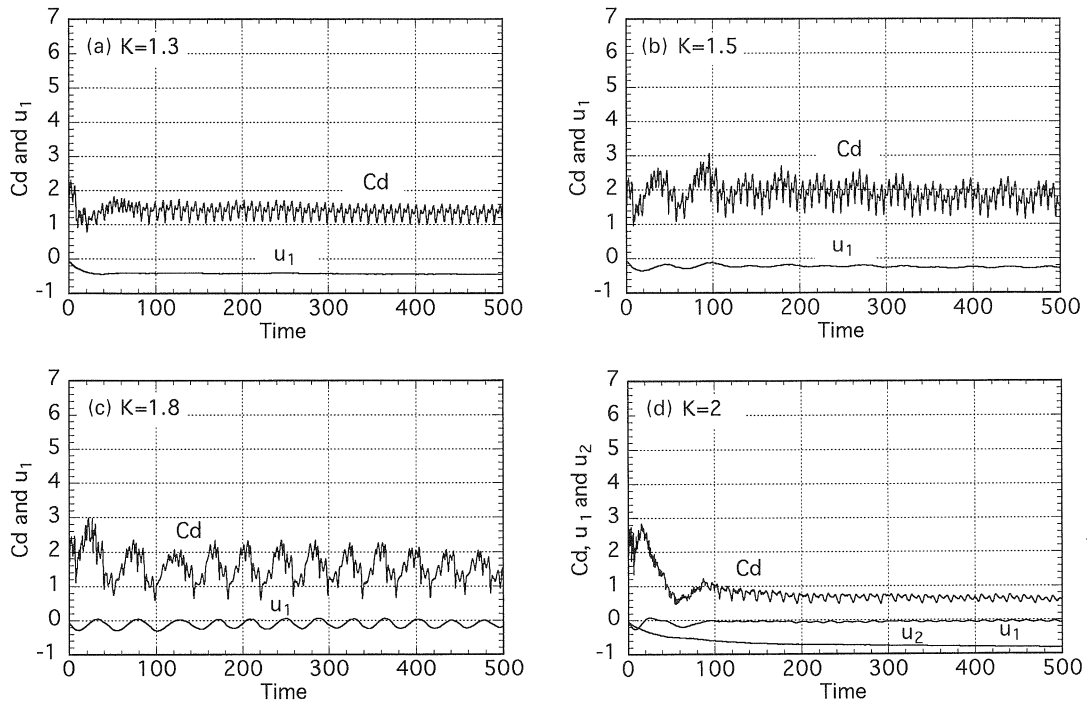

Fig. 22. Time history of drag coefficient C_d on a hill, columnar mode with $n=1$ (u_1) and mode with $n=2$ (u_2) for strong stratification ($1 < K \leqslant 2$), $\mathrm{Re}=2000$.

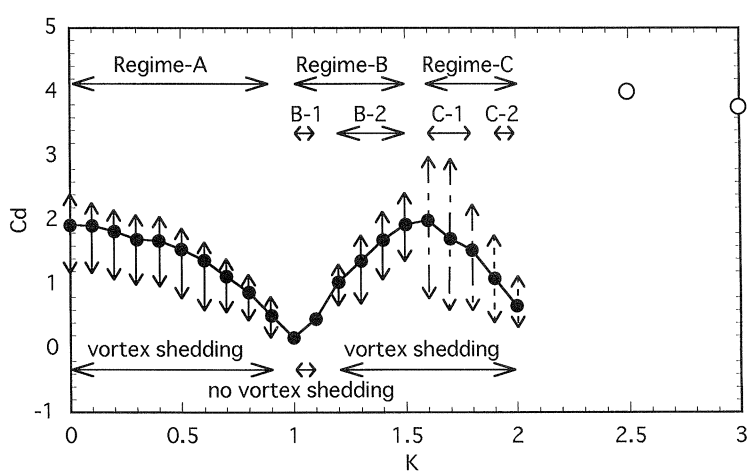

Fig. 23. Variations of drag coefficient C_d on a hill with K ($0 \leqslant K \leqslant 3$), $\mathrm{Re}=2000$. In addition, the flow characteristics around the hill for $0 \leqslant K \leqslant 2$ are summarized. For $K=2.5$ and 3, the flow around a hill becomes complicated.

in which the flow unsteadiness caused by the columnar disturbance can be observed. Furthermore, both Regime-B and Regime-C can be classified into two separate regimes. In Regime B-1, due to the generation of the stationary lee wave with long wavelength, the vortex shedding is strongly suppressed so that the flow around the hill rapidly reaches an almost steady state as time proceeds. In Regime B-2, on the other hand, although the stationary lee wave is excited downstream of the hill, the vortex shedding clearly exists. The flow field that is accompanied by the vortex shedding shows persistent periodic C_d oscillations in Regime C-1 and decaying C_d oscillations in Regime C-2. These flow features for $K \geqslant 1.6$ are almost similar to those observed in the prior numerical results under imposition of a free-slip condition on the ground, both upstream and downstream of the hill, as shown in Fig. 18. However, the only significant difference occurs in the range of K. The flow unsteadiness around the hill is observed over the whole range $1.1 \leqslant K \leqslant 2$ in the prior numerical results, in which persistent periodic oscillations in the C_d are observed for $1.1 \leqslant K \leqslant 1.7$, and decaying C_d oscillations are observed for $1.8 \leqslant K \leqslant 2$.

5. Conclusions

We have performed a direct numerical simulation (DNS) on stably stratified flows over a two-dimensional hill in a channel of finite depth at a Reynolds number of 2000 for a wide range of K ($0 \leqslant K \leqslant 3$). In these simulations, as a first step, we assumed a free-slip condition on the ground, both upstream and downstream of the hill, and imposed a no-slip condition only on the hill surface, much as in the previous towing tank experiments (Castro et al., 1990; Baines, 1995) and numerical studies (Castro, 1989; Hanazaki, 1989a, b; Paisley and Castro, 1994a, Paisley et al., 1994b). Since such a configuration introduces no vortex shedding from the hill, clear-cut characteristics of flows around the hill may be expected.

(1) For strong stratification ($1 < K \leqslant 2$), the present numerical results with $\mathrm{Re} = 2000$ confirmed that the flow around the hill is intrinsically unsteady, which is manifested very clearly as periodic oscillations in the drag coefficient C_d on the hill, and emphasize the following features. The flow unsteadiness is mainly due to the periodic modification in the flow just ahead of the hill. Namely, the flow modification is caused by the periodic shedding of upstream advancing columnar disturbances, which are generated from the hill, of mode $n = 1$ with a clockwise circulation. A low-C_d state corresponds to the situation, in which the columnar disturbance of mode $n = 1$ is just about to detach from the hill, while a high-C_d state corresponds to the situation, in which this disturbance has just detached from the hill. For $1.1 \leqslant K \leqslant 1.7$, columnar disturbances with mode $n = 1$ are dominant so that the flow around the hill shows a persistent periodic unsteadiness. For $1.8 \leqslant K \leqslant 2$, as columnar disturbances with mode $n = 1$ disappear and those with mode $n = 2$ become dominant instead, the flow around the hill rapidly reaches an almost steady state.

(2) There is a significant difference in the normalized periods (UT_1/H) of C_d oscillations between the values predicted by Rottman et al. (1996) (i.e., Eq. (1f)) and those obtained from the present calculations with $\mathrm{Re} = 2000$. Through the calculations with the blockage ratio $H/h = 6, 10$ and corresponding $\mathrm{Re} = 20$, 100 and 2000, it is found that the normalized periods of C_d oscillations for $K = 1.5$ have a strong dependence on both the H/h and Re. At the same blockage ratio, as the Reynolds number decreases, the normalized periods of C_d oscillations tend to reach an almost same value predicted by Eq. (1f). Furthermore, as the blockage ratio becomes larger, the trend in

approaching the predicted value by Eq. (1f) is remarkable at the same Reynolds number, especially for the case with $\mathrm{Re}=2000$. This is likely due to the inhibition of the non-linear effect on the periodic flow unsteadiness around the hill. Therefore, it is reasonable to conclude that in the present numerical results with $H/h=6$ and $\mathrm{Re}=2000$ the non-linear effect can be strongly enhanced, eventually leading to the differences between the predicted values by Eq. (1f). In particular, it is shown that the effect of the blockage ratio is relatively dominant, rather than the Reynolds number in the range $20 \leqslant \mathrm{Re} \leqslant 2000$.

As a next step, in order to investigate the flow around the hill under real atmospheric situations, we have performed calculations under imposition of a no-slip condition on the ground. Under these physical conditions, the Reynolds number was taken to be relatively high so that the unsteady separated–reattached flow behind the hill and the subsequent vortex shedding could be formed. To avoid a troublesome boundary layer effect, we employ a free-slip condition on the ground upstream of the hill, much as in our previous numerical study (Ohya et al., 1992). A no-slip condition is imposed on the hill surface and the downstream of the hill. Particular emphasis is placed on the effect of stable stratifications on the unsteady separated–reattached flow behind the hill.

(3) The flow around the hill exhibits different behavior over the whole range $0 \leqslant K \leqslant 2$, corresponding to the difference in the boundary condition on the ground. For $0 \leqslant K \leqslant 0.9$, the vortex shedding from the separation bubble behind the hill occurs. For $K=1$ and 1.1, the flow around the hill is markedly different from that in the cases of $K=0$–0.9, mainly due to the generation of the stationary lee wave with long wavelength. As time proceeds, the vortex shedding is strongly suppressed so that the flow around the hill rapidly reaches an almost steady state. Under strong stratification ($1 < K \leqslant 2$), although lee waves are excited downstream of the hill, the vortex shedding clearly exists. For $1.2 \leqslant K \leqslant 1.5$, the flow field with a vortex shedding shows an approximately steady state, corresponding to the stationary lee wave. It is much more likely that there is no significant change in the approaching flow just ahead of the hill, because the change in the columnar disturbances with mode $n=1$ is very small. Only when $1.6 \leqslant K \leqslant 2$ does the flow around the hill become unsteady. However, due to the no-slip condition on the ground, the rate of the periodic change in the approaching flow immediately upstream of the hill is remarkably smaller than that of the prior numerical study under imposition of a free-slip condition on the ground, both upstream and downstream of the hill. Accordingly, the rate of the periodic change in the separation bubble is very small. For $K=1.9$ and 2, as columnar disturbances with mode $n=2$ become dominant, the flow around the hill rapidly reaches an almost steady state. These flow mechanisms for $1.6 \leqslant K \leqslant 2$ are almost the same as those discussed in the prior numerical results. The only significant difference occurs in the range of K. The flow unsteadiness around the hill is observed over the whole range $1.1 \leqslant K \leqslant 2$ in the prior numerical results, in which persistent periodic oscillations in the C_d are observed for $1.1 \leqslant K \leqslant 1.7$, and decaying C_d oscillations are observed for $1.8 \leqslant K \leqslant 2$.

References

Baines, P.G., 1979. Observations of stratified flow over two-dimensional obstacles in fluid of finite depth. Tellus 31, 351.

Baines, P.G., 1995. Topographic Effects in Stratified Flow. Cambridge University Press, Cambridge.

Castro, I.P., 1989. Effects of stratification on separated wakes: Part I, weak static stability. Proceedings of the Third IMA Meeting on Stratified Flows, Leeds.

Castro, I.P., Snyder, W.H., Baines, P.G., 1990. Obstacle drag in stratified flow. Proc. R. Soc. London A 429, 119.

Chernyshenko, S.I., Castro, I.P., 1993. High Reynolds number asymptotics of the steady flow through a row of bluff bodies. J. Fluid Mech. 257, 421.

Hanazaki, H., 1989a. Upstream advancing columnar disturbances in two-dimensional stratified flow of finite depth. Phys. Fluids A 1, 1976.

Hanazaki, H., 1989b. Drag coefficient and upstream influence in three-dimensional stratified flow on finite depth. Fluid Dyn. Res. 4, 317.

Janowitz, G.S., 1981. Stratified flow over a bounded obstacle in a channel of finite height. J. Fluid Mech. 110, 161.

Kajishima, T., Ohta, T., Okazaki, K., Miyake, Y., 1997. High-order finite-difference method for incompressible flows using collocated grid system. Bull. Japan Soc. Mech. Eng. B 63–614, 3247 (in Japanese).

Kawamura, T., Takami, H., Kuwahara, K., 1986. Computation of high Reynolds number flow around a circular cylinder with surface roughness. Fluid Dyn. Res. 1, 145.

Kim, J., Moin, P., 1985. Application of a fractional step method to incompressible Navier–Stokes equations. J. Comput. Phys. 59, 308.

Lamb, K.G., 1994. Numerical simulations of stratified inviscid flow over a smooth obstacle. J. Fluid Mech. 260, 1.

Long, R.R., 1953. Some aspects of the flow of stratified fluids. I. A theoretical investigation. Tellus 5, 42.

Long, R.R., 1955. Some aspects of the flow of stratified fluids. III. Continuous density gradients. Tellus 7, 341.

McIntyre, M.E., 1972. On long's hypothesis of no upstream influence in uniformly stratified or rotating flow. J. Fluid Mech. 52, 209.

Ohya, Y., Ozono, S., Matsuo, K., Maeda, A., 1992. Stratified flow over a 2-D semicircular cylinder in fluid of finite depth. Proceedings of the 12th Japan Wind Engineering Symposium, p. 13 (in Japanese).

Paisley, M.F., Castro, I.P., 1994a. A numerical study of wave-breaking in stratified flow over obstacles. Dyn. Atmos. Ocean 23, 309.

Paisley, M.F., Castro, I.P., Rockliff, N.J., 1994b. Steady and unsteady computations of strongly stratified flows over a vertical barrier. In: Stably Stratified Flows. Flow and Dispersion over Topography. Oxford University Press, Oxford, p. 39.

Rottman, J.W., Broutman, D., Grimshaw, R., 1996. Numerical simulations of uniformly stratified fluid flow over topography. J. Fluid Mech. 306, 1.

Turner, J.S., 1973. Buoyancy Effects in Fluids. Cambridge University Press, Cambridge.

Uchida, T., Ohya, Y., 1997. A numerical study of stably stratified flows over a two-dimensional hill. Part I. Free-slip condition on the ground. J. Wind Eng. Ind. Aerodyn. 67 & 68, 493.

Zang, Y., Street, R.L., Koseff, J.R., 1994. A non-staggered grid, fractional step method for time-dependent incompressible Navier–Stokes equations in curvilinear coordinates. J. Comput. Phys. 114, 18.